

Frictional–collisional constitutive relations for granular materials, with application to plane shearing

By P. C. JOHNSON AND R. JACKSON

Department of Chemical Engineering, Princeton University, Princeton, NJ 08544, USA

(Received 31 January 1986)

Within a granular material stress is transmitted by forces exerted at points of mutual contact between particles. When the particles are close together and deformation of the assembly is slow, contacts are sustained for long times, and these forces consist of normal reactions and the associated tangential forces due to friction. When the particles are widely spaced and deformation is rapid, on the other hand, contacts are brief and may be regarded as collisions, during which momentum is transferred. While constitutive relations are available which model both these situations, in many cases the average contact times lie between the two extremes. The purpose of the present work is to propose constitutive relations and boundary conditions for this intermediate case and to solve the corresponding equations of motion for plane shear of a cohesionless granular material between infinite horizontal plates. It is shown that, in general, not all the material between the plates participates in shearing, and the solutions for the shearing material are coupled to a yield condition for the non-shearing material to give a complete solution of the problem.

1. Introduction

The mechanical behaviour of a flowing granular material results from forces exerted at the many points of contact between different particles. These contacts are not permanent, but are continually forming and breaking as the assembly of particles moves. Unless the particle surfaces are perfectly smooth the forces have both tangential and normal components, and the surfaces in contact may, or may not, be slipping relative to each other. When the assembly of particles is widely spaced and in vigorous motion, individual contacts are of short duration and may be treated as ‘collisions’, analogous in many ways to the encounters between molecules in a liquid or gas. For slow deformations at high solids packing density, on the other hand, contacts are semi-permanent, and the normal reaction forces and associated tangential frictional forces at these sliding contacts are dominant. Of course, everything between these extremes is possible and, as we shall see, most situations of practical interest are of this intermediate type. Quite recently (Walton & Braun 1985) some progress has been made towards direct dynamic modelling of the motion of a substantial assembly of particles in situations where mutual contact times may be of arbitrary duration. However, computations of this type are practicable only for simple situations such as plane shear, where periodicity arguments can be used to limit the number of particles whose motion must be followed. To be able to treat more complex situations we must still resort to a continuum model of the particle assembly, with the influence of mutual interactions represented by suitable constitutive relations.

Constitutive models for the high density–slow deformation situation originated in soil mechanics and have quite a long history (Coulomb 1776; Reynolds 1885; Drucker & Prager 1952; Roscoe, Schofield & Wroth 1958; de Jong 1959; Jenike & Shield 1959). With a few exceptions they are not developed from consideration of motions at the ‘microscopic’ scale of individual particles, but are essentially empirical proposals based on plasticity theory or on models of sliding layers that generate frictional forces. More recently the opposite limit of low density–rapid deformation has been treated successfully using ideas of kinetic theory. These originated with Bagnold (1954), who recognized that inertial effects are dominant in momentum transfer under these circumstances. The analogy with the kinetic theory of liquids has been developed for this class of motions by Ackerman & Shen (1982) and by Savage and co-workers (Savage & Jeffrey 1981; Jenkins & Savage 1983; Lun *et al.* 1984), while Haff (1983) independently arrived at similar results by heuristic arguments based on a microscopic view of the particle motion. In this work the kinetic energy of random motion of the grains plays the role of internal energy, with which one may associate a ‘grain temperature’. Since the parameters in the momentum equation are strongly influenced by the value of this grain temperature, the momentum equation must be solved together with a differential balance of the kinetic energy of random motion of the grains. Then the main differences in behaviour between a molecular liquid and a granular material in this regime of motion arise from the fact that collisions are inelastic in the latter case, so that the grain temperature decays to zero unless it is sustained by work done during continued deformation of the grain assembly.

In most situations of practical interest, at least those that are terrestrially based, the compaction of the particle assembly under its own weight is sufficient to ensure that stresses associated with semi-permanent contacts are significant, if not dominant. On the other hand, collisional stresses are rarely insignificant throughout the flow field, so a satisfactory description of the motion requires constitutive relations valid in the difficult case where interparticle contacts are of intermediate duration. In particular, it seems that such a theory is needed for proper interpretation of even the simplest shear experiments, if these extend over a wide range of shear rates (Bagnold 1954; Bridgwater 1972; Savage & Sayed 1984; Hanes & Inman 1985).

The present paper describes a model for motion in this intermediate regime which, while essentially empirical and preliminary in nature, does predict some types of behaviour not found in either of the limiting cases. Rather than attempting to deal directly with particle–particle contacts of intermediate duration, we divide contacts into two classes, long and short, then assume that the former may be treated as semi-permanent frictional contacts, while the latter are treated as inelastic collisions of brief duration. At very low particle volume fractions there will also be significant momentum transfer by translation of particles between adjacent layers, as in the kinetic theory of gases. Thus the total stress transmitted by the particle assembly will be the sum of contributions from these sources, which will be referred to as the ‘frictional’ and the ‘collisional–translational’ contributions respectively.

The question then arises of how these are to be calculated. As mentioned earlier, there exist theories that permit each to be found in the limiting case where it acts alone, but it is not clear how these should be modified to model the intermediate case. For the present, however, we shall simply assume that no modification is necessary; in other words, that the total stress may be approximated as the sum of frictional and collisional–translational contributions, each calculated as if it acted alone. A similar approximation has also been used by Savage (1982) in treating a plane

shearing motion. The result is a curiously hybrid theory, combining an empirical macroscopic model for the frictional stress with a microscopically based model of the collisional–translational stress. Of course, it is unlikely that a truly realistic theory could be as simple as this, but nevertheless it proves possible to solve the resulting equations of motion in simple cases, and hence to investigate the relative roles of the two limiting stress mechanisms. The solutions also show some qualitatively new behaviour which may be characteristic of the intermediate situation.

In this paper the model is applied to the problem of plane shear of an infinite horizontal slab of granular material with bounded thickness. Though simple, this is a system in which gravitational compaction of the material under its own weight is important, provided the applied normal stress is not too large. As a consequence it is shown that the configuration of the steady-state motion may depend on the sequence of operations by which it was established, and that not all the material necessarily undergoes deformation. Shear stress and normal stress are predicted as functions of the overall shear rate, and the relative contributions of frictional and collisional–translational stresses are found as functions of position in the shearing layer.

2. Development of the theory

2.1. Equations of motion

The equations of motion are obtained by combining the differential equations of mass, momentum and energy conservation with the following postulates:

$$\boldsymbol{\sigma} = \boldsymbol{\sigma}_c + \boldsymbol{\sigma}_f, \quad (2.1)$$

$$E = E_{\text{MK}} + E_{\text{PT}} + E_h, \quad (2.2)$$

$$\boldsymbol{q} = \boldsymbol{q}_{\text{PT}} + \boldsymbol{q}_h. \quad (2.3)$$

Here $\boldsymbol{\sigma}$ denotes the total-stress tensor, defined in the compressive sense, while $\boldsymbol{\sigma}_c$ and $\boldsymbol{\sigma}_f$ are the collisional–translational and frictional contributions to the stress respectively. E denotes the total energy per unit mass of the granular material, which is the sum of three components: E_{MK} , the kinetic energy associated with the local average velocity \boldsymbol{u} ($E_{\text{MK}} = \frac{1}{2}\boldsymbol{u}^2$), E_{PT} , the ‘pseudo-thermal’ energy associated with deviations of the motion of individual particles from the local average, and E_h , the true thermal internal energy of the solid material. E_{PT} may be replaced by a ‘grain temperature’ T defined by $E_{\text{PT}} = \frac{1}{2}\overline{v^2} = \frac{3}{2}T$, where $\overline{v^2}$ is the mean square of the velocity fluctuations about \boldsymbol{u} . (Rotational contributions to the pseudo-thermal energy have also been considered by C. K. K. Lun & S. B. Savage 1984, private communication, but are neglected here.) \boldsymbol{q} is the total-energy-flux vector, which is the sum of the true heat flux, \boldsymbol{q}_h , and the flux $\boldsymbol{q}_{\text{PT}}$ of pseudo-thermal energy. The former is related in the usual way to the gradient of thermodynamic temperature and the effective thermal conductivity of the assembly of solid particles, while the latter is similarly related to the gradient in grain temperature, as discussed below.

The balance equation for the true thermal internal energy is taken to be of the form

$$\rho \frac{DE_h}{Dt} = -\nabla \cdot \boldsymbol{q}_h - \boldsymbol{\sigma}_f : \nabla \boldsymbol{u} + I, \quad (2.4)$$

where ρ is the bulk density of the particulate material and D/Dt denotes the material derivative. The term $-\boldsymbol{\sigma}_f : \nabla \boldsymbol{u}$ represents the rate of working of the frictional component of the stress, while I is the rate of dissipation due to the inelasticity of

collisions between particles. Implicit in (2.4) is the assumption that work done by the frictional component of stress is translated directly into thermal internal energy, and does not contribute to the pseudo-thermal energy of the particles.

Using (2.1) in the momentum equation, and subtracting both (2.4) and the mechanical-energy equation from the total-energy equation then leads to the following set of equations of change:

$$\frac{\partial \rho}{\partial t} + \nabla \cdot (\rho \mathbf{u}) = 0, \quad (2.5)$$

$$\rho \frac{D\mathbf{u}}{Dt} = \rho \mathbf{g} - \nabla \cdot (\boldsymbol{\sigma}_c + \boldsymbol{\sigma}_f), \quad (2.6)$$

$$\frac{3}{2} \rho \frac{DT}{Dt} = -\nabla \cdot \mathbf{q}_{PT} - \boldsymbol{\sigma}_c : \nabla \mathbf{u} - I, \quad (2.7)$$

where \mathbf{g} is the specific-gravity force vector. The third of these represents the balance of pseudo-thermal energy, and we see that the rate of working of the collisional-translational component of stress is the source term, while the inelasticity of collisions provides a sink. This reflects our earlier assumption about the form of the true thermal-energy balance. Equation (2.7) is identical with the pseudo-thermal-energy equation postulated by Jenkins & Savage (1983) and by Haff (1983) for the case in which there is no frictional contribution to stress. If the distribution of thermodynamic temperature is needed the above equations must be supplemented by (2.4). This will be necessary, for example, if parameters in the constitutive relations depend significantly on thermodynamic temperature.

The equations of motion must be closed by constitutive equations for $\boldsymbol{\sigma}_c$, $\boldsymbol{\sigma}_f$, \mathbf{q}_{PT} and I , but before discussing these we shall derive the boundary conditions to be satisfied at an interface between the particulate material and a solid surface.

2.2. Boundary conditions

Boundary conditions for \mathbf{u} and T will be developed by arguments similar to those used by Hui *et al.* (1984) for the simpler case in which there are no frictional contributions to the stress.

A condition on the slip velocity between the particulate material and a bounding surface can be obtained by equating the tangential force per unit area exerted on the boundary by the particles to the corresponding stress within the particle assembly close to the boundary. The force per unit area on the boundary is the sum of collisional and frictional contributions. The magnitude of the tangential frictional component will be assumed to be $N_f \tan \delta$, where N_f is the normal frictional component of stress and δ is the angle of friction between the surface and the particulate material. This is simply Coulomb's law of friction applied to the material sliding over the surface. The rate of momentum transfer to unit area of the surface by collisions is the product of the collision frequency for each particle, $(3T)^{1/2}/s$, the average tangential momentum transferred per collision, $\phi' \pi \rho_p d^3 \mathbf{u}_{sl}/6$, and the number of particles adjacent to unit area of the surface, $1/a_c$. Here s denotes the average distance between the boundary and the surface of an adjacent particle, ρ_p is the density of the solid material, d is the particle diameter, \mathbf{u}_{sl} denotes $\mathbf{u} - \mathbf{u}_{wall}$ (the slip velocity), a_c is the average boundary area per particle, and ϕ' is a 'specularity coefficient' whose value depends on the large-scale roughness of the surface and varies between zero for perfectly

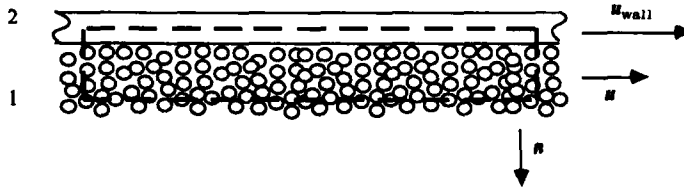


FIGURE 1. Control volume for derivation of the energy-flux boundary condition.

specular collisions and unity for perfectly diffuse collisions. Both s and a_c are functions of the solids volume fraction ν , given by

$$s = d[(\nu_0/\nu)^{\frac{1}{2}} - 1], \quad (2.8)$$

and

$$a_c = d^2(\nu_0/\nu)^{\frac{1}{2}}, \quad (2.9)$$

where ν_0 is the value of ν at closest random packing, assumed to be 0.65 in the present work.

Equating the sum of these frictional and collisional contributions to the component of the bulk stress vector in the direction of u_{sz} then gives

$$\frac{u_{sz} \cdot (\sigma_c + \sigma_f) \cdot n}{|u_{sz}|} + \frac{\phi' \sqrt{3\pi\rho_p} \nu T^{\frac{1}{2}} |u_{sz}|}{6\nu_0 [1 - (\nu/\nu_0)^{\frac{1}{2}}]} + N_f \tan \delta = 0, \quad (2.10)$$

where n is the unit normal from the boundary into the particle assembly. This is the desired condition to be satisfied at the boundary.

The second boundary condition is obtained from energy balances over the control volume shown in figure 1, whose upper and lower faces have unit area and whose depth will be allowed to tend to zero. In this limit the total energy balance and the balance of true thermal energy are then

$$-n \cdot q|_1 - u \cdot (\sigma \cdot n)|_1 + n \cdot q|_2 + u_{wall} \cdot (\sigma_2 \cdot n) = 0 \quad (2.11)$$

and

$$-n \cdot q_h|_1 + n \cdot q_h|_2 + \mathcal{D} - u_{sz} \cdot S_f^b = 0. \quad (2.12)$$

Here σ_2 denotes the stress in the solid material of the bounding wall and S_f^b denotes the frictional force per unit area between the grains and the boundary. \mathcal{D} is the rate of dissipation of pseudo-thermal energy due to inelastic collisions of particles with unit area of the boundary. The last term on the left-hand side of (2.12) represents frictional heating as particles slide over the boundary. Note that $n \cdot \sigma_2 = n \cdot \sigma = S^b$, $q_{PT} = q - q_h$, and that $n \cdot q|_2 = n \cdot q_h|_2$ when the depth of the control volume vanishes, where $S^b = S_c^b + S_f^b$ represents the total force per unit area arising from both friction and collisions between the grains and the boundary. Then subtracting (2.11) from (2.12) gives

$$-n \cdot q_{PT} = \mathcal{D} + u_{sz} \cdot S_c^b, \quad (2.13)$$

where S_c^b is the force per unit area on the boundary due to grain-boundary collisions, as given by the second term on the left-hand side of (2.10). The value of \mathcal{D} is given by the product of the energy loss per particle-boundary collision, the collision frequency per particle and the number of particles adjacent to unit area of the boundary:

$$\mathcal{D} = \left[\frac{1}{2} \pi \rho_p d^3 T (1 - e_w^2) \right] \left[\frac{(3T)^{\frac{1}{2}}}{d[(\nu_0/\nu)^{\frac{1}{2}} - 1]} \right] \left[\frac{1}{d^2(\nu_0/\nu)^{\frac{1}{2}}} \right], \quad (2.14)$$

where e_w is the coefficient of restitution for collisions between particles and the boundary. Substituting for \mathcal{D} from (2.14) into (2.13) and introducing a constitutive expression for \mathbf{q}_{PT} then gives an explicit form for the second boundary condition.

Note that the second term on the right-hand side of (2.13) is negative, and therefore represents a source of pseudo-thermal energy. This term, which was omitted by Hui *et al.* (1984), is included in a more recent derivation of boundary conditions for collisional stresses by Jenkins & Richman (1986). It may be important when slip is large, as we shall see.

2.3. Constitutive relations

The development of constitutive relations for $\boldsymbol{\sigma}_c$, \mathbf{q}_{PT} and I has been the goal of a number of recent studies, starting with the pioneering work of Bagnold (1954). For the present purpose we shall use a modified form of the relations due to Lun *et al.* (1984), making the assumption discussed earlier, that the collisional-translational contribution to stress can be calculated as though it acted in isolation. Then

$$\boldsymbol{\sigma}_c = [\rho T(1 + 4\eta\nu g_0) - \eta\mu_b \nabla \cdot \mathbf{u}] \mathbf{I} - \left(\frac{2 + \alpha}{3} \right) \left\{ \frac{2\mu}{\eta(2 - \eta)g_0} (1 + \frac{8}{5}\eta\nu g_0) [1 + \frac{8}{5}\eta(3\eta - 2)\nu g_0] + \frac{8}{5}\mu_b \eta \right\} \mathbf{S} \quad (2.15)$$

$$\mathbf{q}_{PT} = \frac{-\lambda}{g_0} \left\{ (1 + \frac{12}{5}\eta\nu g_0) [1 + \frac{12}{5}\eta^2(4\eta - 3)\nu g_0] + \frac{64}{25\pi} (41 - 33\eta)(\eta\nu g_0)^2 \right\} \nabla T \\ \times \frac{-\lambda}{g_0} (1 + \frac{12}{5}\eta\nu g_0) \frac{12}{5}\eta(2\eta - 1)(\eta - 1) \frac{d}{d\nu} (\nu^2 g_0) \frac{T}{\nu} \nabla \nu \quad (2.16)$$

and

$$I = \frac{48}{\pi^{\frac{1}{2}}} \eta(1 - \eta) \frac{\rho_p \nu^2}{d} g_0 T^{\frac{3}{2}} \quad (2.17)$$

are the desired relations. Here \mathbf{S} is the deviatoric part of the rate of deformation tensor, and

$$\eta = \frac{1}{2}(1 + e_p), \quad \mu = \frac{5m(T/\pi)^{\frac{1}{2}}}{16d^2}, \quad \lambda = \frac{75m(T/\pi)^{\frac{1}{2}}}{8\eta(41 - 33\eta)d^2}, \quad \mu_b = \frac{256\mu\nu^2 g_0}{5\pi}, \quad (2.18)$$

where m is the mass of a single particle and e_p denotes the coefficient of restitution for collisions between particles. Equations (2.15)–(2.17) differ from the corresponding results of Lun *et al.* in two respects only. First, a multiplicative factor $\frac{1}{3}(2 + \alpha)$ appears in the deviatoric part of $\boldsymbol{\sigma}_c$, where α is a constant of order unity. This factor appeared in the constitutive equations of Jenkins & Savage (1983) but was eliminated in the more complete analysis of Lun *et al.* It is convenient to reintroduce it here to provide one adjustable parameter, though α must tend to unity when e_p and ν approach unity and zero respectively, for consistency with the kinetic theory of dilute gases. Secondly, the Carnahan–Starling form of the radial distribution g_0 is replaced by

$$g_0 = \frac{1}{1 - (\nu/\nu_0)^{\frac{1}{2}}}, \quad (2.19)$$

a form recently used by C. K. K. Lun & S. B. Savage (1984, private communication) which ensures that $g_0 \rightarrow \infty$ when $\nu \rightarrow \nu_0$, and hence constrains ν to remain smaller than ν_0 . It is interesting to note that, when this form for g_0 is inserted into the constitutive equations of Jenkins & Savage (1983), they become essentially equivalent to those of Haff (1983).

While theories of the collisional-translational transport properties are based on micro-structural pictures and kinetic-theory arguments, constitutive models for the

frictional contribution to stress are largely empirical. For example, the 'critical-state' theory of Roscoe *et al.* (1958), Schofield & Wroth (1968), and Roscoe (1970) postulates a nest of yield surfaces in principal-stress space, one for each value of the bulk density of the material. The point on one of these corresponding to a given motion is then identified by the plastic-potential-flow rule, which requires the components of the inward normal to the yield surface at that point to be proportional to the corresponding principal rates of deformation. The constitutive relations are completed by requiring the principal axes of stress and rate of deformation to be aligned, with the major principal rate-of-deformation axis parallel to the minor (compressive) principal stress axis. With these assumptions, specification of the geometry of the nest of yield surfaces completely determines the constitutive relations, and these are of degree zero in the elements of the rate-of-deformation tensor, as required by the rate-independent nature of frictional stresses. Proper choice of geometry for the yield surfaces also describes the dilatation observed by Reynolds (1885) to accompany the deformation of granular materials, and predicts the Coulomb (1776) proportionality between shear and normal stresses in plane shearing. Nevertheless, there are features of frictional stresses that may not be represented properly by models of this type. For example, there is evidence of misalignment of the principal axes of stress and rate of deformation, and other types of theory (e.g. de Jong 1959) do not demand that these should be aligned.

Fortunately, for the present purpose it is not necessary to choose between different theories of the frictional stress, since we are interested only in fully developed plane shear of a non-cohesive material. In this case the material is in a critical state and the shear stress is simply proportional to the normal stress, while the normal stress is related to the bulk density. In fully developed plane shearing, the principal axes of stress are inclined at $\pm \frac{1}{2}\pi$ to the direction of motion, and for the material in a critical state the ratio of principal stresses $\sigma_{\max}/\sigma_{\min} = (1 + \sin \phi)/(1 - \sin \phi)$, where ϕ is known as the internal angle of friction. Then if S_f denotes the frictional contribution to the shear stress and N_f the corresponding contribution to the normal stress, it follows that

$$S_f = N_f \sin \phi. \quad (2.20)$$

We expect N_f to increase rapidly with bulk density and to diverge on approaching the bulk density ν_0 , and a simple algebraic function with this property is

$$N_f = \frac{Fr}{(\nu_0 - \nu)^n}, \quad (2.21)$$

where Fr and n are constants. Arguably the constant ν_0 in this equation may be larger than that represented by the same symbol in (2.19), but we tentatively set them equal to economize in the number of parameters. In accord with our postulate of additivity, the above relations, based on observations of slow shearing, are assumed to carry over unchanged to give the frictional contributions to stress even for more rapid shearing, where collisional stresses also contribute.

3. Plane shear of a granular material

Shear cells, such as those used by Carr & Walker (1967), Bridgwater (1972), Savage & Sayed (1984), and Hanes & Inman (1985) take the form of annular troughs, in which samples of the material are sheared in the vertical plane. Provisions are made for controlling the overall rate of shear and the normal load applied to the sample, and for measuring the shear and normal stresses and the depth of the sample. However,

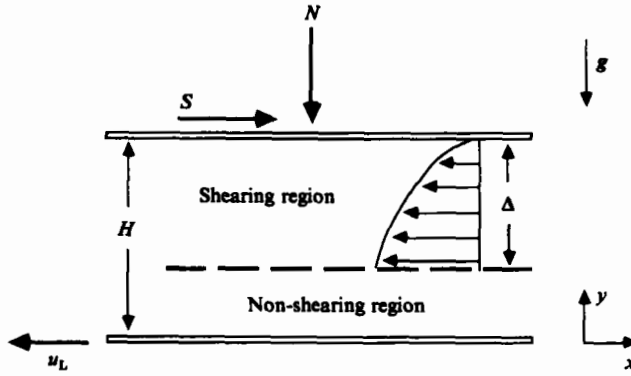


FIGURE 2. Nomenclature for plane shear of a horizontal layer.

velocity and bulk-density profiles within the sample are not measured, so in interpreting the results it has been necessary to assume that the material has uniform properties and is shearing uniformly. As a test of the proposed constitutive relations this situation will be analysed theoretically, and predicted shear and normal stresses will be compared with experimental values. Velocity, bulk-density, and grain-temperature profiles will also be predicted, so it will be possible to examine the validity of the assumption of uniform conditions in the shearing sample.

3.1. Governing equations

For simplicity the annular shear cell will be modelled by plane shear of a horizontal layer, as shown in figure 2. In the general case there may be both shearing and locked zones of grains, and Δ denotes the thickness of the shearing region, but for the moment consider the case in which all the material shears. The motion is fully developed, so all variables depend only on y , a coordinate normal to the plane of shear. Then the two components of the momentum equation and the pseudo-thermal-energy equation, written in terms of a dimensionless mean velocity u^* , grain temperature T^* , spatial coordinate Y , solids volume fraction ν , and frictional normal stress $N_f^*(\nu)$, reduce to

$$1 + B \int_Y^1 \nu \, dY - f_1(\nu) T^* - N_f^*(\nu) = 0, \quad (3.1)$$

$$\frac{d}{dY} \left[AC f_2(\nu) T^{*2} \frac{du^*}{dY} + N_f^*(\nu) \sin \phi \right] = 0 \quad (3.2)$$

and

$$\frac{d}{dY} \left[f_3(\nu) T^{*2} \frac{dT^*}{dY} + f_4(\nu) T^{*2} \frac{d\nu}{dY} \right] + A^2 f_2(\nu) T^{*2} \left(\frac{du^*}{dY} \right)^2 - \frac{f_5(\nu)}{C^2} T^{*2} = 0, \quad (3.3)$$

while the boundary conditions become

$$\frac{dT^*}{dY} = -\frac{f_4(\nu)}{f_3(\nu)} T^* \frac{d\nu}{dY} - \frac{(1 - e_w^2)}{C} f_6(\nu) T^* + \frac{\phi' A^2}{C} f_7(\nu) u^{*2} \quad (3.4)$$

and

$$\frac{du^*}{dY} = -\frac{\phi' f_8(\nu) u^*}{C} + \frac{D}{AC} \frac{N_f^*(\nu)}{f_2(\nu) T^{*2}}, \quad (3.5)$$

$$\begin{aligned}
 f_1(\nu) &= \nu[1 + 4\eta\nu g_0(\nu)], \\
 f_2(\nu) &= \frac{(2 + \alpha) 5\pi^{\frac{1}{2}}}{288\eta(2 - \eta)} \left(\frac{1}{g_0(\nu)} + \frac{2}{3}\eta\nu \right) [1 + \frac{2}{3}\eta(3\eta - 2)\nu g_0(\nu)] + \frac{8\eta\nu^2 g_0(\nu)(2 + \alpha)}{15\pi^{\frac{1}{2}}}, \\
 f_3(\nu) &= \frac{25\pi^{\frac{1}{2}}}{16\eta(41 - 33\eta)} \left\{ \left(\frac{1}{g_0(\nu)} + \frac{12\eta\nu}{5} \right) [1 + \frac{12}{5}\eta^2(4\eta - 3)\nu g_0(\nu)] + \frac{64}{25\pi} (41 - 33\eta)\eta^2\nu^2 g_0(\nu) \right\}, \\
 f_4(\nu) &= \frac{25\pi^{\frac{1}{2}}}{16\eta(41 - 33\eta)} \left(\frac{1}{\nu g_0(\nu)} + \frac{12}{5}\eta \right) \frac{1}{2}\eta(2\eta - 1)(\eta - 1) \frac{d}{d\eta} (\nu^2 g_0(\nu)), \\
 f_5(\nu) &= \frac{48}{\pi^{\frac{1}{2}}} \eta(1 - \eta)\nu^2 g_0(\nu), \\
 f_6(\nu) &= \frac{\pi\sqrt{3\nu g_0(\nu)}}{4\nu_0 f_3(\nu)}, \\
 f_7(\nu) &= \frac{\pi\nu g_0(\nu)}{2\sqrt{3\nu_0 f_3(\nu)}}, \\
 f_8(\nu) &= \frac{\pi\nu g_0(\nu)}{2\sqrt{3\nu_0 f_0(\nu)}}.
 \end{aligned}$$

TABLE 1. Dimensionless functions

to be satisfied at $Y = 1$, together with

$$\frac{dT^*}{dY} = -\frac{f_4(\nu)}{f_3(\nu)} T^* \frac{d\nu}{dY} + \frac{(1 - e_w^2)}{C} f_6(\nu) T^* - \frac{\phi' A^2}{C} f_7(\nu) (u^* + u_L^*)^2 \tag{3.6}$$

and

$$\frac{du^*}{dY} = \frac{\phi' f_8(\nu)}{C} (u^* + u_L^*) + \frac{D}{AC} \frac{N_t^*(\nu)}{f_2(\nu) T^{*2}}, \tag{3.7}$$

to be satisfied at $Y = 0$. Here the dimensionless velocity, grain temperature, spatial coordinate, and frictional normal stress are defined by

$$u^* = \frac{u}{u_L}, \quad T^* = \frac{\rho_p T}{N}, \quad Y = \frac{y}{A}, \quad N_t^*(\nu) = \frac{N_t(\nu)}{N}, \tag{3.8}$$

where N is the total normal stress applied to the upper plate, and u_L is the velocity of the lower plate. The dimensionless functions $f_1(\nu)$ to $f_8(\nu)$ are defined in table 1, while the dimensionless parameters A – D are given by

$$A = \left(\frac{\rho_p u_L^2}{N} \right)^{\frac{1}{2}}, \quad B = \frac{\rho_p g A}{N}, \quad C = \frac{d}{A}, \quad D = \tan \delta - \sin \phi, \tag{3.9}$$

Equations (3.4)–(3.7) come from the boundary conditions (2.10) and (2.13). The equations of motion now contain the following dimensionless parameters: A/d , ν , $\rho_p u_L^2/N$, $\rho_p g A/N$, e_p , e_w , ϕ , δ , ϕ' , and $F\tau/N$. In view of their number a complete exploration of the parameter space is not practicable, and we shall be content with solutions for a limited set of conditions corresponding to experiments reported in the literature.

The problem defined by (3.1)–(3.7) can be solved analytically when $\rho_p g A/N \ll 1$, $e_w = 1$, and no-slip conditions are imposed in place of (3.5) and (3.7) at the boundaries. The first of these conditions requires the weight of the sample to be small compared

with the normal load applied to the upper plate, so that the total normal stress on horizontal planes is approximately constant throughout the sample. The remaining two eliminate both generation and dissipation of pseudo-thermal energy at the boundaries, and hence ensure that the flux of pseudo-thermal energy vanishes throughout the sample. Then T^* and ν are independent of Y , and are determined algebraically by

$$T^* = \frac{A^2 C^2 f_2(\nu)}{f_5(\nu)} \quad (3.10)$$

and

$$\frac{A^2 C^2 f_1(\nu) f_2(\nu)}{f_5(\nu)} + N_f^*(\nu) = 1, \quad (3.11)$$

while the velocity profile is linear,

$$u^*(Y) = Y - u_L^*. \quad (3.12)$$

Finally, the ratio of shear to normal stress is given by

$$\frac{S}{N} = A^2 C^2 \left[\frac{f_2^3(\nu)}{f_5(\nu)} \right]^{\frac{1}{2}} + N_f^*(\nu) \sin \phi. \quad (3.13)$$

If the shearing mass M_s per unit horizontal area is given, together with the thickness of the shear layer Δ , then ν is determined, and (3.11) and (3.13) show that both S and N are proportional to $(u_L/\Delta)^2$ at high shear rates. Equation (3.10) shows that the grain temperature is then also proportional to the square of the shear rate.

For other parameter values the equations must be solved numerically. The derivative of (3.1) provides a relation between $d\nu/dY$ and dT^*/dY which can be used to eliminate $d\nu/dY$ from the remaining equations and boundary conditions. Nonlinear terms in the resulting equations are then linearized about approximate value of ν , u^* and T^* , and derivatives are replaced by finite-difference approximations, yielding a set of linear equations in the unknown values of u^* and T^* at the grid points. These are solved to generate new approximations to these variables; then (3.1) is solved for the new approximation to ν . This whole process is then iterated to convergence. The numerical results have been checked against the analytical solution described above, and for grids of 11, 21, 31 and 41 points the two agree to within 1%. The changes in computed values of S/N and the mean volume fraction of solids are less than 0.5% for a change from 11 to 31 grid points, but the changes in the computed u^* and T^* profiles are somewhat larger. Accordingly 11 grid points are used when only the stress and the mean bulk density are required, but a 31-point grid is introduced whenever profiles within the sample are required. With the 11 point grid an average of twenty-five iterations is needed for convergence.

The solution procedure requires values for N , Δ , u_L , and the physical properties ρ_p , e_p , e_w , d , ϕ , δ and ϕ' . Profiles of u^* , T^* and ν are then generated, while the shearing mass per unit area and the shear stress are determined from

$$M_s = \rho_p \Delta \int_0^1 \nu \, dY \quad (3.14)$$

and

$$\frac{S}{N} = A C f_2(\nu) T^{*2} \frac{du^*}{dY} + N_f^*(\nu) \sin \phi. \quad (3.15)$$

3.2. Plane shear with complete shearing

We shall first assume that the whole of the material between the upper and lower plates is shearing ($\Delta = H$), and examine the consequences of this in relation to

available experimental measurements. Then M_s is equal to the specified total mass M_T of granular material between unit area of the plates.

Unfortunately, the solution procedure described at the end of the last section does not correspond to the conditions imposed in experiments. These are of two kinds. In constant-load experiments the sample mass and the applied normal stress are held constant, while the shear stress and the depth of the sample vary as the overall rate of shear is changed. In constant-volume experiments, on the other hand, both the mass per unit area and the depth of the sample are held constant, while the normal load and the shear stress change in response to changes in the overall shear rate. In the former case, therefore, a solution must be found by iterating on the value of H to match the specified value of M_T , while in the latter case the specified M_T is matched by iterating on the value of N .

Of the published experimental studies using annular shear cells only that of Savage & Sayed (1984) gives sufficient details of the experimental procedure to permit a reasonably unambiguous comparison with our theoretical predictions. These authors made measurements of the constant-volume type by the following procedure. The lower plate was rotated while the upper plate was loaded to apply a known normal stress and restrained from rotating by a torque measuring device, which determined the shear stress. The speed of rotation was then adjusted until the total depth of the sample was such as to give the desired value of the mean bulk density. The load on the upper boundary was then changed through a sequence of values, and after each change the speed of rotation was adjusted until the sample depth resumed its former value, when the shear stress was recorded. This sequence was traversed for both increasing and decreasing values of the normal load.

To match the experiments of Savage & Sayed theoretical calculations were performed for samples of 0.0018 m diameter glass beads and 0.001 m diameter polystyrene beads. The values of d , ϕ and ρ_p for these materials were given by Savage & Sayed, but estimates had to be made for ϕ' , δ , e_p , e_w , Fr and n . The surfaces of the experimental cell were lined with rough sandpaper and, if this is assumed to have the same roughness as a layer of the beads themselves, the corresponding value for δ is $\tan^{-1}(\sin \phi)$. The coefficients of restitution, e_p and e_w , were estimated roughly by measuring the height of rebound when glass and polystyrene beads were dropped onto glass, polystyrene and sandpaper-covered surfaces. The specular coefficient ϕ' was arbitrarily assigned the reasonable value 0.6. Experiments of Scarlett & Todd (1969) indicate that the critical-state bulk density is almost independent of applied normal load for materials of the sort considered here, so the exponent n in (2.21) must be large, and a value of 40 was chosen for both materials. Note that, while experimental values for some of the above physical parameters were provided by Savage & Sayed, others were not, and for these estimated 'reasonable values' were utilized. Nevertheless, no attempt was made to adjust these values to obtain a better fit between theory and experiment for the shear tests. The estimated values were retained throughout the calculations. Only two parameters were determined by fitting experiments, namely Fr and α . The value for Fr was adjusted until the predicted value of M_s equalled the experimental value, for a single experimental set of values of u_L , N and Δ . This value of Fr was subsequently retained in all calculations referring to the same material. The complete set of physical-property and parameter values for each material is recorded in table 2. The only remaining parameter in the theory is α , which appears in (2.15). This was assigned the value 1.6 since a value of unity led to predictions of shear stresses that were rather low in comparison with measured values. There was no attempt to adjust the value of α for the different materials.

Property	Glass beads	Polystyrene beads
d	0.0018 m	0.001 m
e_p	0.80	0.87
e_w	0.50	0.50
Fr	$3.65 \times 10^{-32} \text{ kg m}^{-1} \text{ s}^{-2}$	$4.0 \times 10^{-32} \text{ kg/m}^{-1} \text{ s}^{-2}$
n	40	40
M_T	16.52 kg m^{-2}	3.95 kg m^{-2}
α	1.60	1.60
δ	22.9°	22.9°
ϕ	25.0°	25.0°
ϕ'	0.60	0.60
ϕ_y	25.2°	24.7°
ρ_p	2980 kg m^{-3}	1095 kg m^{-3}

TABLE 2. Sample properties

Figures 3 and 4 compare calculated normal and shear stresses with the experimental measurements, for glass and polystyrene beads respectively. In both cases the agreement is good for the normal stresses, which become proportional to the square of the overall shear rate when this is large. For the glass beads the predicted shear stress agrees quite well with observations at the largest value of the mean volume fraction $\bar{\nu}$, but the predictions fall progressively below the observations as $\bar{\nu}$ decreases. Measured values of the shear stress for the polystyrene beads are very scattered, but the same behaviour of the predictions is discernible there.

The results for the polystyrene beads raise a further question. As noted above, the measurements of S/N are rather scattered; nevertheless there is a clear trend of increasing S/N as u_L is increased, while in contrast the theoretical predictions decrease with increasing u_L , just as they do for the glass beads. However, this is not an inherent feature of the theory. Thus it is easy to see that the analytical solution, found in §3.1, predicts that S/N is independent of u_L in the absence of frictional stresses ($Fr = 0$), and by taking $Fr \neq 0$ it is not difficult to find solutions for which S/N increases with u_L . It is therefore possible that an alternative choice of parameter values for the polystyrene beads would resolve this discrepancy. Indeed, better agreement between theory and experiment could undoubtedly have been obtained by regarding all parameters not specified by Savage & Sayed as adjustable, but this would have been inappropriate, since they are not, in principle, adjustable parameters, but could be determined by suitable measurements independent of the shear test.

Figure 5(a, b) shows predicted profiles of velocity and grain temperature in the sample of glass beads, at the highest experimental bulk density, and for three different values of the overall shear rate. From figure 5(a) the slip velocities at both boundaries are seen to increase with increasing shear rate, as expected, and the velocity profile becomes more nearly linear. At the lowest shear rate, on the other hand, the profile is strongly curved, and the material near the lower boundary is hardly shearing at all. Figure 5(b) shows that the grain temperature increases on moving into the material from each boundary, so in these conditions the boundaries act as sinks for pseudo-thermal energy. At the lowest overall shear rate the grain temperature is very low near the bottom of the sample, where we have already noted that the local shear rate almost vanishes. Profiles of ν are not shown, since the strong dependence of N_f on ν ensures that the requisite balances can be satisfied with only small variations in the bulk density.

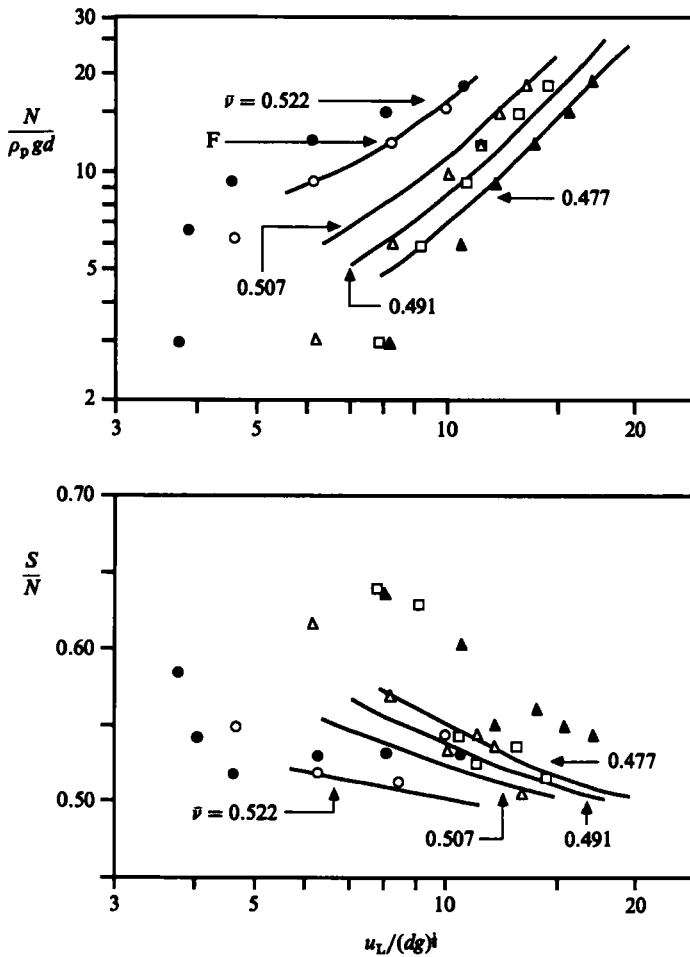


FIGURE 3. Predictions of the complete shearing analysis compared with constant- $\bar{\nu}$ experiments of Savage & Sayed (1984) using 0.0018 m diameter glass beads. Experimental results: ●, $\bar{\nu} = 0.522$ (increasing load); ○, 0.522 (decreasing load); △, 0.507; □, 0.491; ▲, 0.477. The arrow F indicates the datum point used to determine Fr .

In figure 5(c) the ratio of the collisional-translational normal stress to the total normal stress is shown, and it is seen that most of the normal load is borne by this component in the region of highest grain temperature. However, the frictional component increases rapidly with depth and is the larger of the two in all cases near the lower boundary. Indeed, as might be expected from the grain-temperature profile, at the smallest shear rate the collisional-translational component contributes very little to the total stress near the lower boundary. The increase in the frictional contribution on moving down through the sample is a consequence of gravitational compaction due to the increasing overburden of the granular material itself. This is particularly important when the normal stress applied to the upper plate is comparable with the weight of the sample, as is the case here. The curves of figure 5(c) show that theories based entirely on frictional stresses, or entirely on collisional-translational stresses, are inadequate throughout the range of conditions spanned by the experiments.

The theoretical curves in figures 3 and 4 do not extend to such small values of

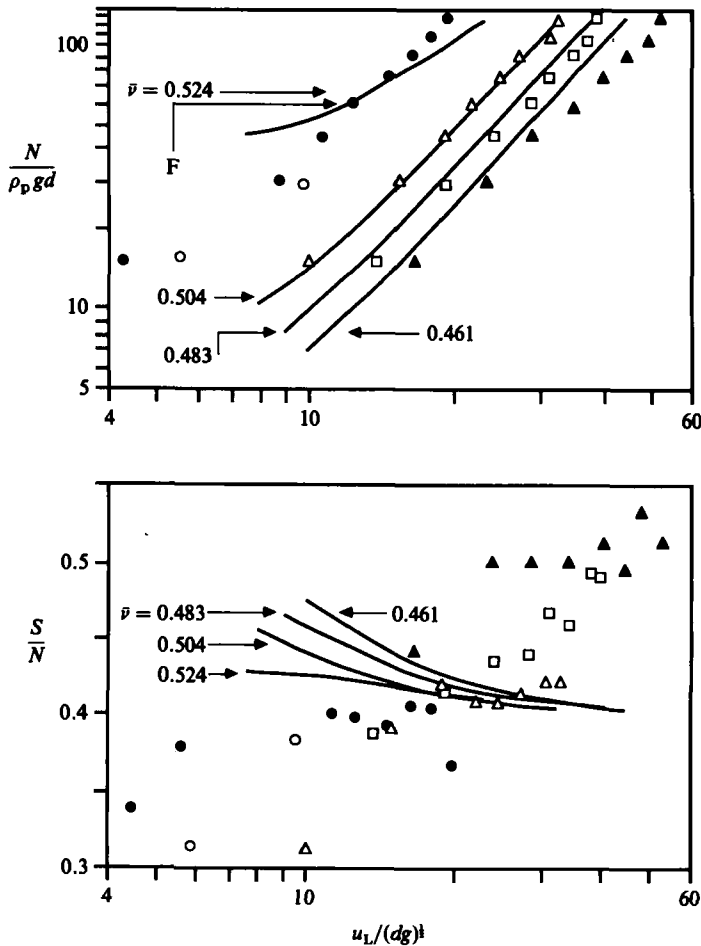


FIGURE 4. Predictions of the complete shearing analysis compared with constant- $\bar{\nu}$ experiments of Savage & Sayed (1984) using 0.001 m diameter polystyrene beads. Experimental results: ●, $\bar{\nu} = 0.524$ (increasing load); ○, 0.524 (decreasing load); △, 0.504; □, 0.483; ▲, 0.461. The arrow F indicates the datum point used to determine $\bar{F}r$.

$u_L/(gd)^{1/2}$ as the experimental points. This is no accident of plotting, but reflects the fact that, for each value of $\bar{\nu}$, there is a minimum value of the overall rate of shear below which acceptable solutions do not exist in a layer of the depth specified. The reason for this is gravitational compaction, as a consequence of which the total normal stress increases with increasing depth, though the total shear stress must remain constant throughout the layer. At low overall shear rates not only the total normal stress but also its frictional component increases on moving down, so the frictional component of the shear stress must also increase. Then, to maintain the constancy of the total shear stress, there must be a compensating decrease in the collisional-translational component. But this cannot decrease beyond zero without a reversal in sign of the velocity gradient du^*/dY and, while solutions of the equations of motion exhibiting such a reversal are possible, they do not represent physically acceptable behaviour. Instead the material no longer shears below the level at which du^*/dY reaches zero. If there is no yielding the shear stress is free to take values smaller than the product of the normal stress and $\sin \phi$, so maintaining a constant

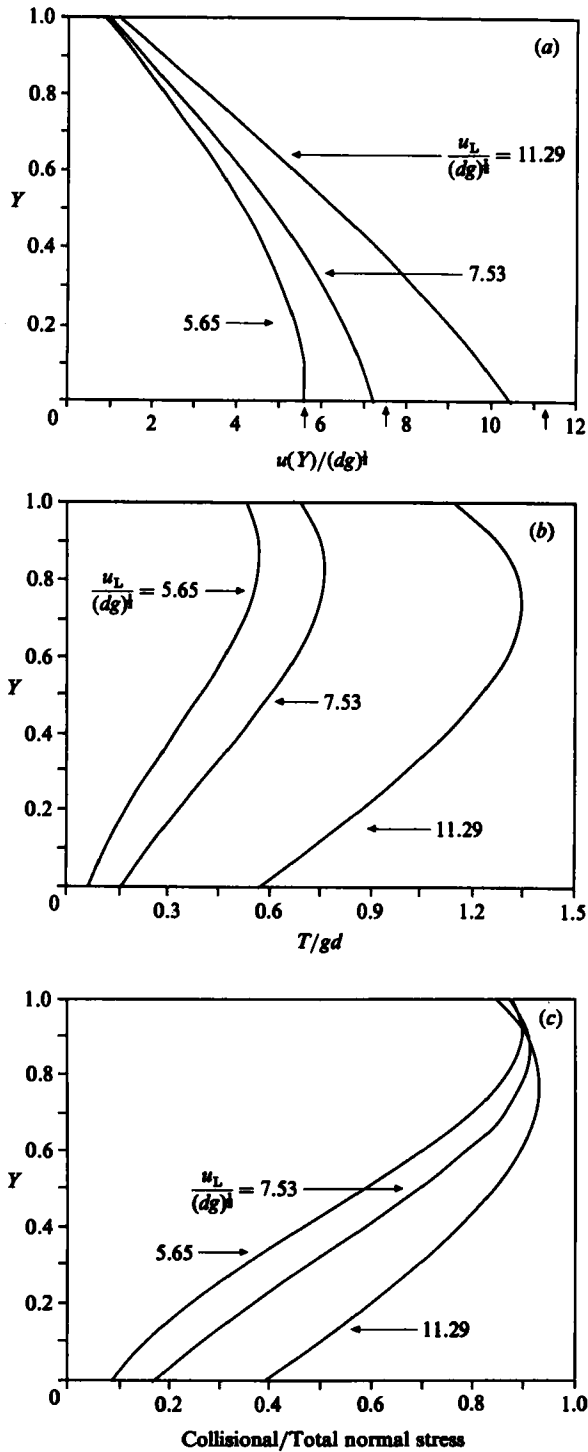


FIGURE 5. (a) Predicted velocity profiles for the sample of glass beads with $\bar{\nu} = 0.522$. Parameter values from table 2. Arrows indicate values of the abscissa corresponding to the lower-plate velocity. (b) Predicted grain-temperature profiles for the sample of glass beads with $\bar{\nu} = 0.522$. Parameter values from table 2. (c) Predicted ratios of the collisional component of normal stress to the total normal stress for the sample of glass beads with $\bar{\nu} = 0.522$. Parameter values from table 2.

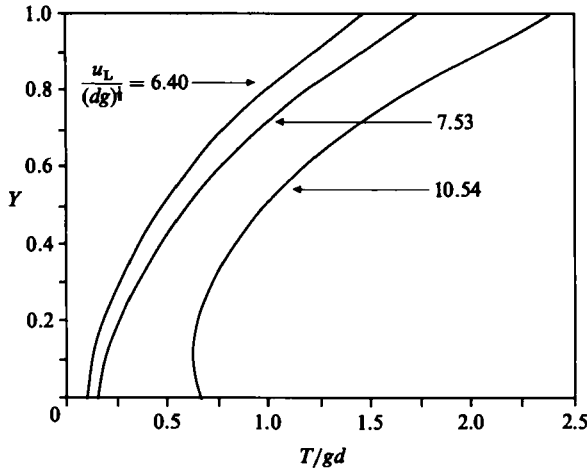


FIGURE 6. Predicted grain-temperature profiles for the sample of glass beads with $\bar{\nu} = 0.522$. Parameter values from table 2, except that $e_w = 0.90$ and $Fr = 2 \times 10^{-37} \text{ kg/ms}^2$.

shear stress despite continued increases in normal stress presents no problem. When $\tan \delta \leq \sin \phi$ the critical condition that identifies the minimum value of u_L is the vanishing of du^*/dY at $Y = 0$, so figure 5(a) shows the minimum value of $u_L/(dg)^{\frac{1}{2}}$ to be approximately 5.65 for the sample of glass beads with $\bar{\nu} = 0.522$. This corresponds to the terminus of the $\bar{\nu} = 0.522$ curves in figure 3. Note that the experimental points extend to smaller values of the overall shear rate and turn downward quite sharply below the termini of the theoretical curves. In this region we expect that only part of the sample is shearing; a situation that will be examined in the next section.

In figure 5(a) the slip between the granular material and the lower plate is seen to vanish when du^*/dY vanishes at $Y = 0$. This is not generally the case but results from the choice $\tan \delta = \sin \phi$ in this example. For values of $\tan \delta < \sin \phi$, there is a non-vanishing slip velocity at the lower plate for the minimum u_L .

As noted earlier the grain-temperature profiles of figure 5(b) indicate that the boundaries act as sinks of pseudo-thermal energy. However, this is not always so. Figure 6 shows the results of calculations for the glass beads, using the parameter values of table 2, except that e_w is increased to 0.9, while Fr is decreased to $2 \times 10^{-37} \text{ kg m}^{-1} \text{ s}^{-2}$. The value of $\bar{\nu}$ is 0.522, so the results may be compared with those in figure 5(b). With the more elastic boundaries it is seen that there is a net generation of pseudo-thermal energy at the upper boundary in all cases. Because of gravitational compaction the lower boundary remains a sink except at the highest shear rate, when $u_L/(dg)^{\frac{1}{2}} = 10.54$. However, in this case both boundaries act as sources and, correspondingly, the collisional-translational contribution to the stress increases once more on approaching the lower boundary.

We have already explored some effects of changing the values of δ and e_w . Of the remaining parameters e_p is not easy to measure, yet might be expected to have a significant influence on the theoretical predictions. To examine this some calculations were repeated for the glass beads, with parameter values from table 2, except that e_p was increased to 0.85, with a compensating change in Fr so that the predictions still fitted the single selected experimental point. The results for two values of $\bar{\nu}$ are shown in figure 7, from which it is seen that all the curves are steeper with the larger

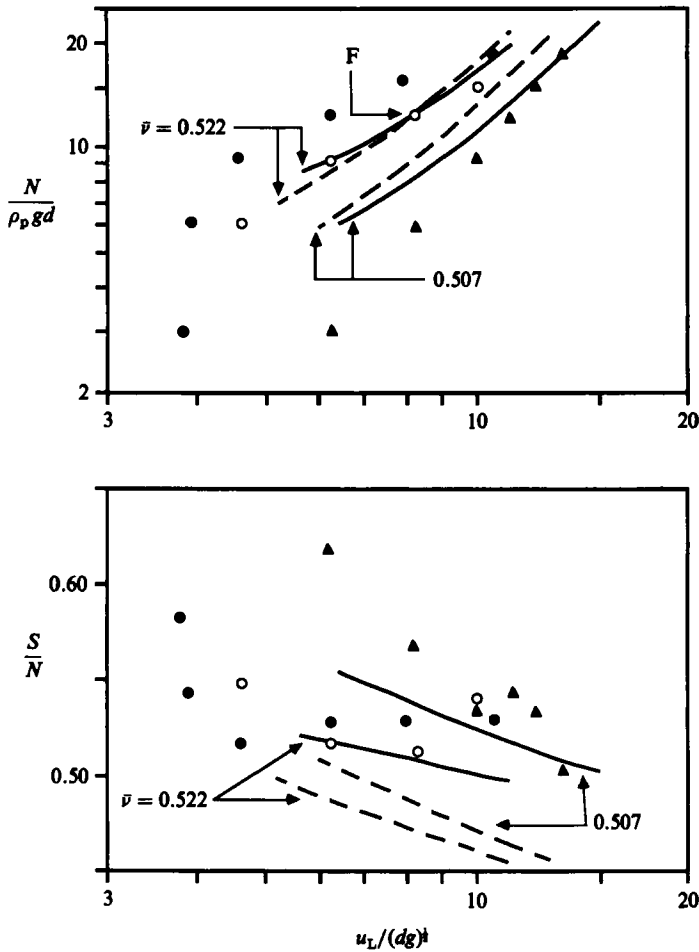


FIGURE 7. Effect of the value of e_p on predicted stresses for the sample of glass beads: —, predictions with $e_p = 0.80$; ---, predictions with $e_p = 0.85$. All other parameter values from table 2, except for $\bar{F}r$, which is adjusted so that the normal stress curves still pass through point F. Experimental results: ●, $\bar{\nu} = 0.522$ (increasing load); ○, 0.522 (decreasing load); ▲ = 0.507.

value of e_p . In addition, values of S/N are reduced by about 10% and the curves extend to smaller values of u_L when e_p is increased.

3.3. Plane shear allowing for partial shearing of the sample

Though it was assumed in the last section that the entire sample had somehow evolved from a well-compacted rest state into the dilated steady-shearing state, it is possible, owing to the yield strength of the material at rest, that a fully shearing state is never achieved. Thus Hanes & Inman (1985), viewing the grains through the transparent walls of their shear cell, observed distinct shearing and non-shearing layers over certain ranges of values of the applied normal load and the overall shear rate. In this section we shall combine our above analysis of plane shear with a yield model for the non-shearing material to predict the response of the granular sample to motion of its boundaries, without assuming that all the material between these boundaries must necessarily be shearing.

Figure 2 depicts the situation that will be analysed. A total mass M_T per unit

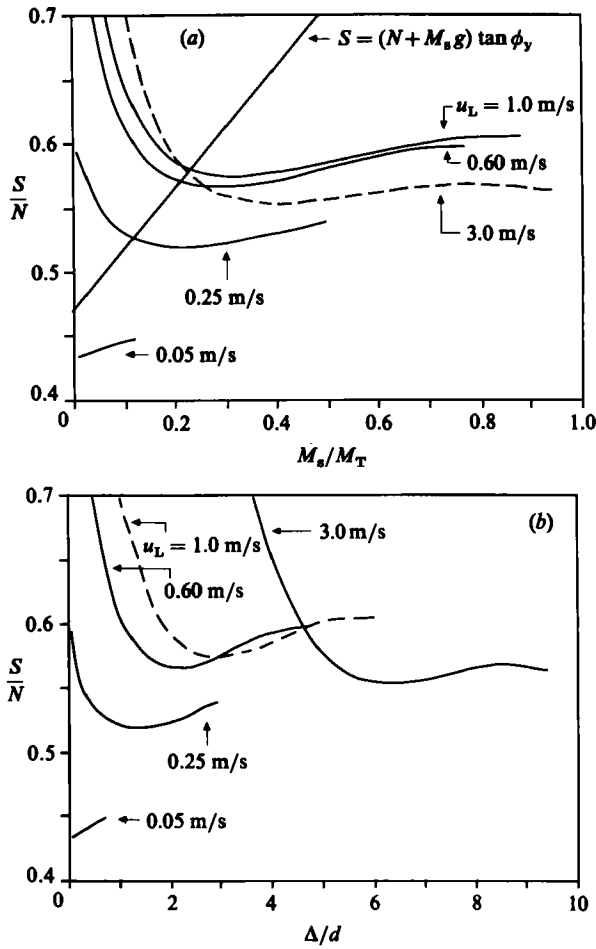


FIGURE 8. Predicted relation between shear stress and (a) M_s/M_T , (b) Δ/d for the sample of glass beads with various values of u_L and a constant normal stress of 160 kg/ms^2 applied to the upper plate.

cross-sectional area is loaded into the gap between the upper and lower plates, and a constant normal stress N is applied to the upper plate, while the lower plate is constrained not to displace vertically. The lower plate is driven at a constant speed u_L , while tangential motion of the upper plate is restrained by a shear stress S . The goal of the analysis is then to predict the kinematics of motion of the material between the plates, the vertical separation between the plates, and the shear stress S , as functions of u_L and N . In particular, it is required to predict the existence, location, thickness and structure of both shearing and non-shearing layers.

For this purpose we must first model the yield behaviour of the granular material, and we shall take the simplest view that it behaves as a cohesionless Coulomb material, for which the shear stress at yield is proportional to the normal stress. Thus $S = N \tan \phi_y$ at yield, where ϕ_y is the angle of friction at *initial yield*. Note that this is not the same as the angle ϕ in (2.20), which determines the ratio of the shear stress to normal stress for a layer in *fully developed* shear, where the material is everywhere at a critical state. ϕ_y depends on the density of packing of the material, while ϕ is independent of bulk density in a simple critical-state model.

The sequence of configurations adopted by the granular material as u_L increases depends on the nature of its initial packing between the plates, so this must be specified fully. In the present calculations we shall assume that the material is packed at uniform volume fraction ν_1 , large enough to correspond to an overconsolidated state even at the lower plate, where the normal stress is largest. Then ϕ_y takes a constant value throughout the sample, and $\tan \phi_y > \sin \phi$. Since the normal stress is smallest at the upper plate, the shear stress for yield is also smallest there, so with the above assumptions shear will be initiated in a layer adjacent to the upper plate, as indicated in figure 2. For the computations ν_1 is assumed to be 0.58 and the values selected for ϕ_y , which are given in table 2, were obtained from initial yield experiments on similar materials. They are such that $\tan \phi_y$ is slightly larger than $\sin \phi$. These values are largely arbitrary, and consequently the results of the analysis should be regarded as indicative of the nature of the behaviour to be expected, rather than predictions for quantitative comparisons with experimental results.

Within the shearing layer the theory of §3.2 applies, but the thickness Δ of this layer is not known *a priori*. However, recalling the computational procedure that led to (3.14) and (3.15), for given N and u_L we may specify a value of Δ , then find profiles of u , T and ν , and calculate the mass per unit area M_s within the shearing layer and the ratio S/N . Repeating this for a sequence of values of Δ gives M_s/M_T and S/N as functions of Δ ; then Δ may be eliminated between these to give S/N as a function of M_s/M_T . The results of such computations, for the glass-bead sample whose properties are given in table 2, can be found in figure 8(a), where curves of S/N are shown for various values of u_L , at a fixed value $160 \text{ kg m}^{-1} \text{ s}^{-2}$ for the applied normal stress. Figure 8(b) shows the same results using Δ/d as the independent variable. In these computations the lower boundary of the shearing layer is the surface of the undeformed lower layer of granular material, which is treated as a solid boundary with $e_w = e_p$, $\tan \delta = \sin \phi$, and $\phi' = 0.6$. The curves intersect the axis $M_s/M_T = 0$ at increasing values of S/N as u_L is increased. Also each curve terminates at some upper value of M_s/M_T and, by examining the complete set of curves, this is seen to have two consequences: first, for each value of u_L there is a maximum mass per unit area that can be maintained in shear and, secondly, for each value of M_s/M_T there is a minimum value of u_L below which all the material cannot be maintained in shear. This feature has already been encountered in the calculations of §3.2, and is attributed to gravitational compaction. Note also that, for a fixed value of M_s/M_T , S/N may not be a monotone function of u_L . Indeed, for M_s/M_T greater than about 0.23, S/N can be seen first to increase, then decrease, as u_L is increased.

The boundary of the shearing layer must now be located using the condition that the shear stress should match the yield stress for the material at the top of the undisturbed lower layer. Since the normal stress at the top of the lower layer is $N + M_s g$, the yield value of the shear stress there is $(N + M_s g) \tan \phi_y$, which is represented by the straight line in figure 8(a).

For illustrative purposes let us now consider the following experiment: the sample of glass beads described by table 2 is assembled between the plates with initially uniform volume fraction $\nu_1 = 0.58$, which corresponds to an initial plate separation $H_0/d = 5.31$. The lower plate is then driven at a speed of 0.05 m/s. From figure 8(a) the curve for $u_L = 0.05 \text{ m/s}$ does not intersect the yield line, so no material shears in these conditions. Correspondingly, the overall dilatation is zero, and $H = H_0$. The reason for this behaviour is that $\tan \delta < \tan \phi_y$, so friction between the slowly moving plate and the surface of the granular material is insufficient to cause the material to yield. If u_L is now increased to 0.25 m/s the added contribution of collisional

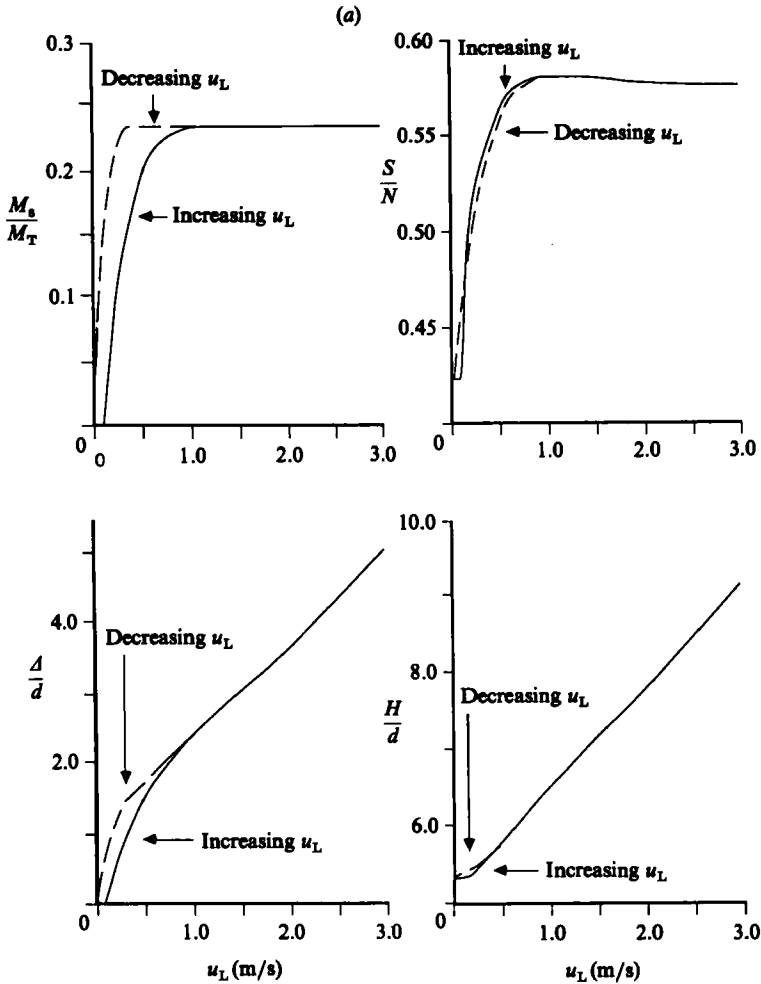


FIGURE 9(a). For caption see facing page.

components of the stress causes the curve to intersect the yield line at a point corresponding to $M_s/M_T = 0.12$, and figure 8(b) then shows that Δ/d is 0.75. The corresponding overall dilation is given by $H/d = 5.42$. As u_L continues to increase the shear stress also increases at constant M_s , so more material enters the shearing layer, as dictated by the intersections of the curves in figure 8(a) with the yield line. This continues until $u_L \approx 1$ m/s, but then a further increase in u_L at constant M_s causes a decrease in the shear stress, which drops below the value determined by the yield line. Clearly then, this increase in u_L cannot force any more material to enter the shear layer. Nevertheless, there is no reason why any of the material already shearing should cease to do so, and M_s/M_T now remains constant as u_L increases further, while S/N decreases. Thus there is a finite mass of material per unit area that can be induced to shear, no matter how large the lower-plate velocity, and this is seen from figure 8(a) to correspond to $M_s/M_T \approx 0.23$.

Now suppose u_L is decreased after having reached a large value via the sequence of changes just described. Since conditions in the shearing layer start from a point below the yield line for the material at the top of the lower layer, M_s does not change initially. Furthermore, scrutiny of figure 8(a) shows that S never increases beyond

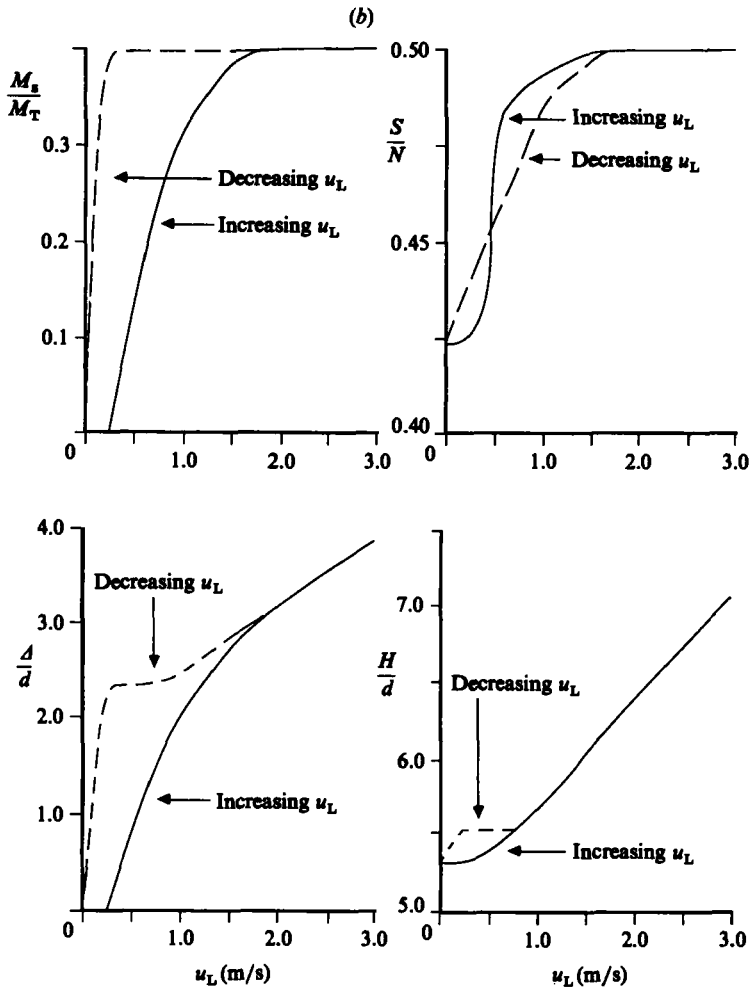


FIGURE 9. The effect of changes in u_L on various properties of the sample of glass beads, with a constant normal stress of (a) $160 \text{ kg m}^{-1} \text{ s}^{-2}$ and (b) 1000 kg/ms^2 applied to the upper plate.

the value defined by the yield line, so no new material is ever drawn into the shear layer. However, somewhere between $u_L = 0.25 \text{ m/s}$ and 0.05 m/s the curves cease to extend to values of M_s/M_T as large as 0.23, and when this happens material that was previously shearing must redeposit on the upper surface of the non-deforming layer. Then M_s/M_T decreases with further decreases in u_L , following the termini of the successive curves in figure 8(a).

The response of the system to the sequence of changes described above is shown in figure 9(a), where curves of M_s/M_T , S/N , A/d and H/d are plotted, for both increasing and decreasing values of u_L . Though there is a marked hysteresis in M_s/M_T and A/d , this is not reflected very strongly in the externally measured quantities S/N and H/d . Figure 9(b) gives the same information for a second sequence of conditions which differ from the first only in the value of the applied normal stress N , which is increased to $1000 \text{ kg m}^{-1} \text{ s}^{-2}$. The pattern of behaviour is the same as before, but now the hysteresis effects are much more pronounced.

It is interesting that the limitation on the thickness of the shearing layer is not

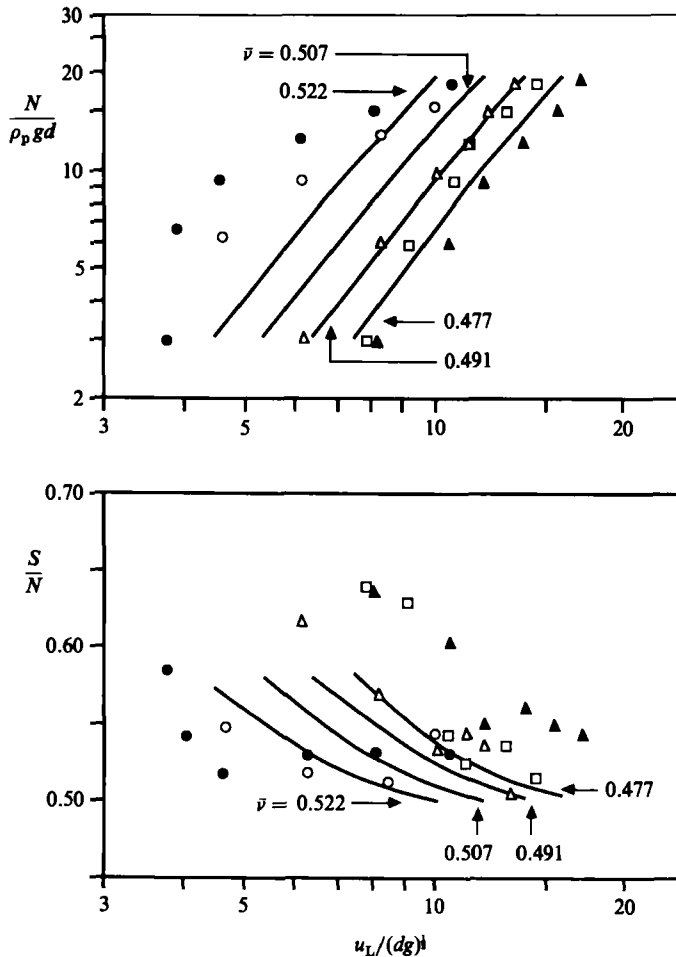


FIGURE 10. Predictions of the partial shearing analysis compared with constant- $\bar{\nu}$ experiments of Savage & Sayed (1984) using 0.0018 m diameter glass beads. Parameter values from table 2. Experimental results: ●, $\bar{\nu} = 0.522$ (increasing load); ○, 0.522 (decreasing load); △, 0.507; □, 0.491; ▲, 0.477.

a simple phenomenon, but is imposed by different features of the mechanics of the system over different ranges of the independent variables. As u_L first increases from zero the shear stress is insufficient to cause the granular material to yield, and there is no shear layer. When the shear layer begins to grow as u_L increases beyond these small values, the factor that limits the amount of material it may contain is the yield strength of the undisturbed material. With further increase in u_L this amount reaches a constant maximum value, which is determined by the condition that the shear stress begins to decrease, rather than increasing, for a small increase in u_L at constant M_s . Finally, when u_L is decreased once more to sufficiently small values, the amount sheared decreases as u_L is decreased. This is a consequence of the fact that the constant- u_L curves terminate at finite values of M_s/M_T , which decrease with u_L . The largest value attainable for M_s/M_T depends on the applied normal stress, and is quite limited. Thus, when $N = 160 \text{ kg m}^{-1} \text{ s}^{-2}$, figure 9(a) shows that only about 23% of the material can be sheared, no matter how large the value of u_L . From figure 9(b), this fraction increases to about 40% when N is raised to $1000 \text{ kg m}^{-1} \text{ s}^{-2}$.

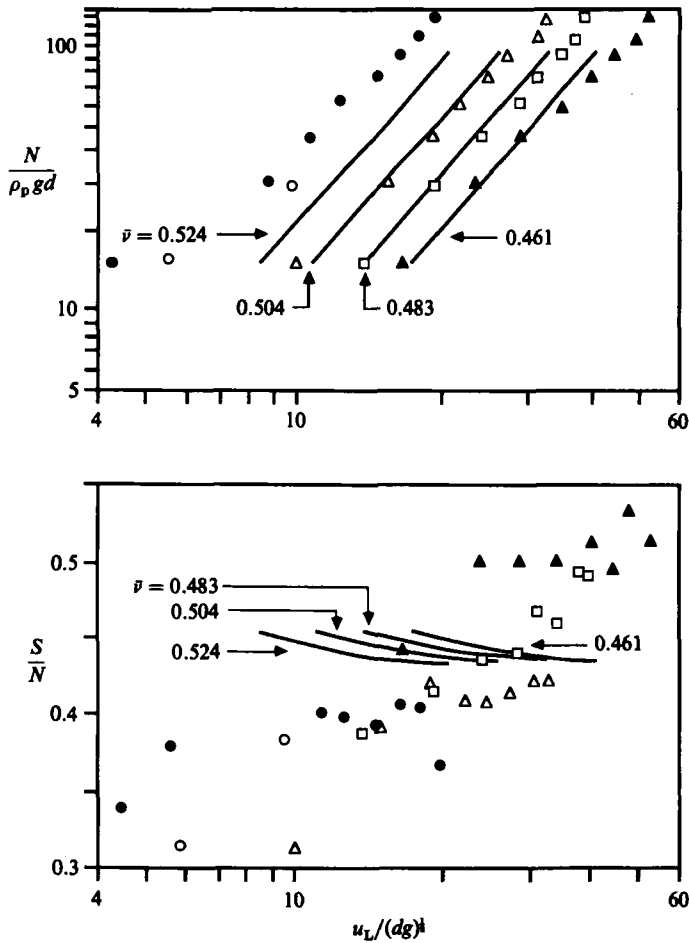


FIGURE 11. Predictions of the partial shearing analysis compared with constant- $\bar{\nu}$ experiments of Savage & Sayed (1984) using 0.001 m diameter polystyrene beads. Parameter values from table 2. Experimental results: ●, $\bar{\nu} = 0.524$ (increasing load); ○, 0.524 (decreasing load); △, 0.504; □, 0.483; ▲, 0.461.

In terms of the particle size, the limiting shear-layer thicknesses correspond to 2.3 and 3.0 particle diameters respectively, for the light and heavy applied normal loads. The validity of a continuum approach is certainly questionable for such thin shearing depths, and finite-particle effects would undoubtedly need to be taken into account should one want to model quantitatively such shearing motions. The partial-shearing analysis should not be dismissed as being meaningless, however, because it describes a systematic approach to determine the growth of a shearing zone from a rest state, and quite minor modifications of the theory which serve to increase the collisional contribution to stress, such as changes in the radial distribution function, could also increase the predicted thickness of the shear layer substantially. The qualitative predictions provide us with a description of the importance of yielding and stress generation mechanisms, as well as indicating the need for more detailed experimental reports of the sample preparation and the shear test procedure. The predicted thin shear layers are a result of both the physical nature of the shear test and the predictive capabilities of the theory. Theory predicts shear stresses that are too low to induce

substantial yielding in the overconsolidated sample, while the geometry of the shear cell is such that the influence of gravity limits the maximum shear thickness to ≈ 7 particle diameters (for typical applied normal loads) even if the yield strength of the material is neglected, as has been observed in all reported annular-shear-cell experiments.

We must emphasize, once more, that the above results refer specifically to a situation in which the granular material is initially at a uniform bulk density that corresponds everywhere to an overconsolidated condition. Different patterns of initial packing lead to different patterns of behaviour in the shear test. For example, suppose that the material was initially packed at a uniform density that corresponded to an underconsolidated condition under the applied normal stress, even at the upper plate. Then it is not difficult to see that the first response to an increasing shear stress is yield of a thin layer of material in contact with the *lower* plate. This layer compacts and strengthens as it yields, so deformation soon ceases. Further increases in the applied shear stress cause yielding and compaction of other layers, each just above the previously compacted one. With continued increase in shear stress, therefore, there is continued growth of a layer of material adjacent to the lower plate, with uniform yield strength that always matches the applied shear stress. When this stress reaches the yield stress corresponding to the normal stress N applied to the upper plate, the whole sample has been brought to a condition of uniform yield strength (but not uniform density), and further increases in the shear stress simply cause matching increases in this strength as a result of compaction of all the material. This process continues until the shear stress reaches a value $N \sin \phi$, at which point the material in the uppermost layer is in a critical state, and sustained lateral relative motion of the plates becomes possible. An infinitely thin layer adjacent to the upper plate is then shearing, and no further change can be induced by continued slow shearing. However, if the rate of shear is now increased, collisional-translational stresses contribute and a shearing layer of finite thickness develops adjacent to the upper plate, while below this the material compacts to a new yield strength that matches the total shear stress in the shearing layer. Continuing increases in the rate of shear cause more material to enter the shearing layer and, at the same time, the yield strength of the non-shearing layer increases to match the total shear stress, while remaining spatially uniform. The spatial configuration is similar to that in the first case, for which detailed calculations have been reported, but now the whole lower layer has a uniform yield strength and is, therefore, at incipient yield, while the bulk density varies with depth.

From this discussion it is clear that a definitive interpretation of experimental test results is not possible unless the experimenters have provided details of the procedure by which the test sample was prepared. Nevertheless it is interesting to simulate the experiments of Savage & Sayed without the restrictive assumption of total shearing that was previously invoked. Lacking any detailed information about the initial packing of the test sample, we have assumed it to have uniform overconsolidated bulk density, so quantitative comparisons of theory and experiment should not be taken too seriously. All the parameter values used in generating figures 3 and 4 are retained in these calculations.

The partial-shearing calculations already described [figures 8 and 9] predict H/d , for a fixed value of N , when u_L is varied, whereas the experimental procedure varies N and u_L in order to keep H/d constant. An analogous procedure may be followed computationally, iterating on the value of N for each u_L until H equals the desired H/d . The results of such calculations are shown in figures 10 and 11 for the glass and

polystyrene beads respectively, together with Savage & Sayed's experimental points. These diagrams should be compared with figures 3 and 4, which show the corresponding results for the calculations that assume total shearing. At first sight the agreement between theory and experiment does not seem to be improved by allowing for partial shearing, but closer scrutiny reveals that the curves in figures 10 and 11 extend down to the smallest values of u_L used in the experiments, rather than terminating at some higher value where it ceases to be possible to shear the whole sample. Furthermore, the normal-stress curves in figures 3 and 4 become less steep as u_L decreases, in contrast to the experimental points which turn downward more steeply. The normal-stress curves of figures 10 and 11, on the other hand, maintain the steepness of their slope down to the smallest values of u_L . Thus the qualitative trends of the experimental data are better represented by the analysis that allows for partial shearing.

Separate curves for increasing and decreasing u_L are not shown in figures 10 and 11, though the results of figure 9(*a, b*) indicates that hysteresis will be present. The computed curves for the two cases lie so close together that they are indistinguishable on the scale of the diagrams, so our inclusion of partial shearing does not account for the marked hysteresis observed experimentally at the highest value of the bulk density.

It is remarkable that a continuum theory gives fairly sensible predictions of results from an experimental apparatus in which the total depth of the sample is only six or seven particle diameters, and only a fraction of this material is expected to shear. It would be desirable to compare the theory with measurements on much thicker samples, under conditions in which the shear layers are also expected to be thicker. This could be achieved by decreasing the density of the solid material, using higher values of the applied normal load, or working in a gravity-free environment.

4. Concluding remarks

The constitutive relations proposed combine the contributions of frictional and collisional-translational mechanisms for stress transmission to represent the intermediate situation, in a way that is essentially arbitrary but has the virtue of simplicity. Furthermore, it introduces no extra parameters in addition to those belonging to theories of the two separate limiting cases. Predictions of the behaviour of granular materials in plane shear are fairly close to the available experimental data but, in view of the preliminary nature of the theory and the lack of information regarding parameter values for the experimental materials, quantitative comparisons are probably less useful than qualitative similarities between observed and calculated behaviour. In particular, the analysis of §3.3 indicates that much more detailed documentation of experimental procedures will be needed for unambiguous theoretical interpretation. It is important that all relevant properties of both particles and solid boundaries should be measured independently of the shear tests, that the method of assembling the sample and the complete sequence of subsequent changes in applied stress and apparent shear rate should be recorded and, if possible, that the apparatus should be constructed in a way which permits the sample to be observed so as to ascertain which part of it is actually shearing.

To describe a shear test correctly it is clear that a good constitutive theory for the shearing material is not enough. A proper description of the yield properties of non-deforming material is also needed, and the interaction between shearing and non-shearing material at their mutual interface must be understood. In the present

paper this last point has been dismissed by assuming that the interface can be treated like a solid boundary, with appropriate values of the angle of friction, coefficient of restitution and specularly factor. Then the boundary conditions proposed in §2.2 describe the influence of the non-shearing material on the adjacent shearing material. However, we have neglected any effect of the interaction on the non-shearing material itself. In view of the flux of pseudo-thermal energy to the interface this is certainly an oversimplification. It seems likely that pseudo-thermal energy will be conducted into the non-shearing material, reducing its yield strength, and the extent of this reduction will also be influenced by the properties of the solid surface that constitutes the second boundary of the non-shearing layer.

Regardless of its degree of success in describing plane shear, or any other motion of a granular material, a theory of the present type can only be regarded as an expedient substitute for a proper treatment of particle-particle contact interactions of a dissipative nature, with arbitrary duration.

This work is supported by the United States Department of Energy under Grant No. DE-FG22-84PC70803. It also forms part of a larger programme on various aspects of the motion of particulate systems, which is supported by the National Science Foundation, Multiphase and Interfacial Phenomena Program, under Grant No. CBT-8504201.

REFERENCES

- ACKERMAN, N. L. & SHEN, H. 1982 Stresses in rapidly sheared fluid-solid mixtures. *J. Engng Mech. Div. ASCE* **108**, 95-113.
- BAGNOLD, R. A. 1954 Experiments on a gravity-free dispersion of large solid spheres in a Newtonian fluid under shear. *Proc. R. Soc. Lond. A* **225**, 49-63.
- BRIDGWATER, J. 1972 Stress-velocity relationships for particulate solids. *ASME paper no. 72-MH-21*.
- CARR, J. F. & WALKER, D. M. 1967 An annular shear cell for granular materials. *Powder Tech.* **1**, 369-373.
- COULOMB, C. A. 1776 Essai sur une application des règles de maximis et minimis à quelques problèmes de statique, relatifs à l'architecture. *Acad. R. Sci. Mém. Math. Phys. par Divers Savants* **7**, 343-382.
- DE JONG, G. DE J. 1959 Statics and kinematics in the failable zone of granular material. Thesis, University of Delft.
- DRUCKER, D. C. & PRAGER, W. 1952 Soil mechanics and plastic analysis or limit design. *Q. Appl. Maths.* **10**, 157-165.
- HAFF, P. K. 1983 Grain flow as a fluid-mechanical phenomenon. *J. Fluid Mech.* **134**, 401-430.
- HANES, D. M. & INMAN, D. L. 1985 Observations of rapidly flowing granular-fluid materials. *J. Fluid Mech.* **150**, 357-380.
- HUI, K., HAFF, P. K., UNGAR, J. E. & JACKSON, R. 1984 Boundary conditions for high-shear grain flows. *J. Fluid Mech.* **145**, 223-233.
- JENIKE, A. W. & SHIELD, R. T. 1959 On the plastic flow of Coulomb solids beyond failure. *Trans. ASME E: J. Appl. Mech.* **26**, 599-602.
- JENKINS, J. T. & RICHMAN, M. W. 1986 Boundary conditions for plane flows of smooth, nearly elastic, circular disks. *J. Fluid Mech.* **171**, 53-69.
- JENKINS, J. T. & SAVAGE, S. B. 1983 A theory for the rapid flow of identical, smooth, nearly elastic, spherical particles. *J. Fluid Mech.* **130**, 187-202.
- LUN, C. K. K., SAVAGE, S. B., JEFFREY, D. J. & CHEPURNIY, N. 1984 Kinetic theories for granular flow: inelastic particles in Couette flow and slightly inelastic particles in a general flow field. *J. Fluid Mech.* **140**, 223-256.

- REYNOLDS, O. 1885 On the dilatancy of media composed of rigid particles in contact. *Phil. Mag.* **20**, 469–481.
- ROSCOE, K. H. 1970 The influence of strains in soil mechanics. *Géotechnique* **20**, 129–170.
- ROSCOE, K. H., SCHOFIELD, A. N. & WROTH, C. P. 1958 On the yielding of soils. *Géotechnique* **8**, 22–53.
- SAVAGE, S. B. 1982 Granular flows down rough inclines – review and extension. In *Proc. of U.S.–Japan Seminar on New Models and Constitutive Relations in the Mechanics of Granular Materials* (ed. J. T. Jenkins & M. Satake). Elsevier.
- SAVAGE, S. B. & JEFFREY, D. J. 1981 The stress tensor in a granular flow at high shear rates. *J. Fluid Mech.* **110**, 225–272.
- SAVAGE, S. B. & SAYED, M. 1984 Stresses developed by dry cohesionless granular materials sheared in an annular shear cell. *J. Fluid Mech.* **142**, 391–430.
- SCARLETT, B. & TODD, A. C. 1969 The critical porosity of free flowing solids. *Trans. ASME B: J. Engng Ind.* **91**, 477–488.
- SCHOFIELD, A. N. & WROTH, C. P. 1968 *Critical State Soil Mechanics*. McGraw-Hill.
- WALTON, O. R. & BRAUN, R. L. 1985 Viscosity, granular-temperature and stress calculations for shearing assemblies of inelastic frictional disks. *Quarterly Technical report for U.S. DOE, contract number W-7405-Eng-48*, 25 June.